Journal of Materials Chemistry A

β-Functionalized Push-Pull Opp-Dibenzoporphyrins as Sensitizers for Dye-Sensitized Solar Cells: The Role of the Phenylethynyl Bridge

Journal:	*Journal of Materials Chemistry A*
Manuscript ID	TA-ART-02-2019-001846.R1
Article Type:	Paper
Date Submitted by the Author:	15-Mar-2019
Complete List of Authors:	Hu, Yi; University of North Texas, Chemistry Webre, Whitney; University of North Texas, Department of Chemistry Thomas, Michael; University of North Texas, Department of Chemistry Moss, Austen; University of North Texas Hancock, Sarah; University of North Texas Schaffner, Jacob; University of North Texas D'Souza, Francis; University of North Texas, Chemistry Wang, Hong; University of North Texas, Chemistry

Journal Name

ARTICLE

β-Functionalized Push-Pull *Opp*-Dibenzoporphyrins as Sensitizers for Dye-Sensitized Solar Cells: The Role of the Phenylethynyl Bridge

Received 00th January 20xx,
Accepted 00th January 20xx

DOI: 10.1039/x0xx00000x

www.rsc.org/

Yi Hu,[a‡] Whitney A. Webre,[a‡] Michael B. Thomas,[a] Austen Moss,[a] Sarah Hancock,[a] Jacob Schaffner,[a] Francis D'Souza *[a] and Hong Wang *[a]

A novel class of β-functionalized push-pull zinc *opp*-dibenzoporphyrins was designed and synthesized as sensitizers for dye-sensitized solar cells. Dibenzoporphyrin **YH7** displayed strong push-pull characteristics, which included clearly segregated HOMO/LUMO and fast charge injection from the singlet excited state of zinc porphyrin to the conduction band of TiO_2. The incorporation of both phenylethynyl bridge and amino group was critical to achieve the enhanced push-pull effect. The highest PCE value in this series was obtained with the **YH6** cell at 6.7%, which is comparable to that of the best ruthenium dye, **N719** (η = 7.4%), under similar conditions. The high PCE of the **YH6** cell is ascribed to its high light harvesting ability and favorable cell kinetics, which is supported by electrochemical impedance spectral studies and femtosecond transient absorption studies. An unusual illumination-induced photodegradation was observed for **YH7**, which was attributed as the major reason that caused the unexpected lower PCE of the **YH7** cell (η = 5.7%). This work demonstrates the applicability of π-extended porphyrins as a new generation of sensitizers for high performance dye-sensitized solar cells.

1. Introduction

Research on Dye-Sensitized Solar Cells (DSSCs) has attracted intense attention in the past decade due to the rising awareness of the global energy crisis.[1] Porphyrins possess favorable properties as sensitizers for DSSCs, including multiple absorption bands in the visible region and appropriate cell kinetics for electron injection and charge recombination. However, solar cells based on porphyrin dyes had suffered low efficiencies (η < 7.2%) for more than a decade.[2] The introduction of *meso*-functionalized push-pull porphyrins in 2009 by the Diau and Yeh group completed changed the profile of porphyrins in DSSC.[3] Porphyrins have recently stood out as the most promising dyes among all other organic compounds.[4] Significant efforts have been devoted to developing push–pull porphyrin dyes as well as other organic dyes in the past few years, record-breaking power conversion efficiencies (PCEs) have been achieved with porphyrin-based DSSCs in recent years.[5] However, problems still exist with porphyrin dyes. Solar cell instability caused by labile anchoring groups,[6] lengthy synthetic routes, and lower photostability constitute major barriers preventing the utilization of porphyrin dyes in practical applications.

In order to address these problems, new classes of porphyrin dyes should be developed. Porphyrin dyes can be mainly classified into two main types: *meso*-functionalized and β-functionalized. Significant efforts have been devoted to developing *meso*-functionalized porphyrin dyes, which led to the best organic dyes for DSSCs.[5a,d,e,7] In contrast, β-functionalized porphyrin dyes have only been sporadically investigated due to synthetic difficulties.[8] Even less studied are β-functionalized π-extended porphyrins.[9] π-Extended porphyrins possess broadened and red-shifted absorption bands, which enable better overlap with the solar spectrum.[10]

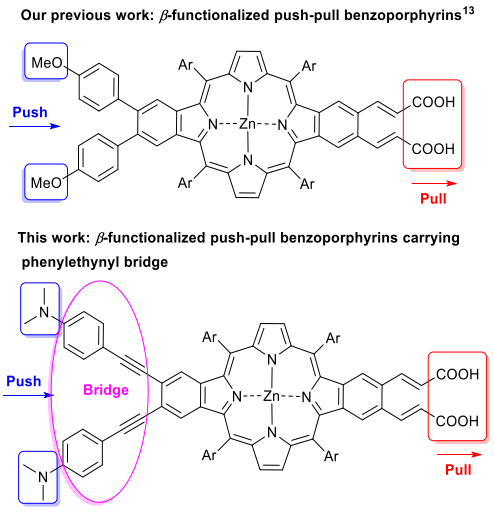

Figure 1 Structure of β-functionalized push-pull π-extended porphyrins

[a] Department of Chemistry, University of North Texas, 1155 Union Circle, #305070, Denton, TX 76203-5017, USA
‡ equal contributions
*Email: hong.wang@unt.edu; francis.dsouza@unt.edu
Electronic Supplementary Information (ESI) available: See DOI: 10.1039/x0xx00000x

As such, the development of π-extended porphyrins may provide new opportunities for dye-sensitized solar cells.

Our group has been engaged in developing β-functionalized push-pull benzoporphyrins as sensitizers for DSSCs in recent years.[11] To design these porphyrin sensitizers, we utilize the existing push-pull design strategy, which has played a pivotal role in improving the PCEs of porphyrin dyes.[6a,b,8h,12] Additionally, we take advantage of concise and versatile synthetic methodologies developed for benzoporphyrins in our laboratory, and install two vicinal linker groups on the porphyrin to enhance the binding between the dye and TiO_2 surface.[6d]

In a previous work,[13] we prepared a class of push-pull dibenzoporphyrins (Figure 1, top). While these types of porphyrins showed enhanced PCEs as compared with their monobenzoporphyrin analogues,[11a] significant push-pull effects were not observed. This is mainly due to the steric congestion at the porphyrin β, β'-positions, causing the phenyl rings to be perpendicular to the plane of the porphyrin core, and thus limited the electronic communication of the push group (methoxy group) with the porphyrin core. In order to further enhance the PCE and, very importantly, investigate the impact of the push-pull effect of dibenzoporphyrins on power conversion efficiency, we have designed a new class of push-pull dibenzoporphyrins in which a phenylethynyl bridge is inserted between the push group (tertiary amine) and the porphyrin core, to alleviate the steric crowding around the porphyrin periphery (Figure 1, bottom). Herein, we present the synthesis, structure-property studies of these β-functionalized push-pull *opp*-dipenzoporphyrins and their evaluation as sensitizers in DSSCs.

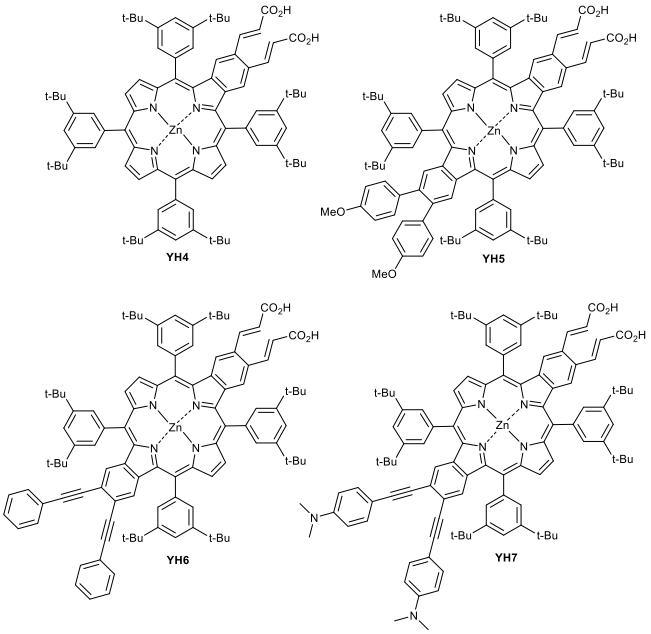

Figure 2 β-functionalized push-pull *opp*-dibenzoporphyrins studied in this work

2. Results and discussion

2.1 Molecular design and synthesis

In this work, we have designed two new *opp*-dibenzoporphyrins (**YH6**–**YH7**) (Figure 2). The incorporation of the phenylethynyl bridge is expected to alleviate the steric congestion at the porphyrin periphery to allow strong electronic communication between the push group and the porphyrin core. In addition, the incorporation of an ethynyl spacer will also further extend the π-conjugation, resulting in broadened and red-shifted absorption bands. In both porphyrins, acrylic acid serves a dual purpose as both the pull and anchoring group. Our previous work has shown that acrylic acid is the best anchoring group for benzoporphyrin dyes as compared to carboxylic acid, benzoic acid, and ethynylbenzoic acid.[11a] In porphyrin **YH7**, tertiary amine groups serve as the push group. Porphyrin **YH6** does not contain tertiary amine groups in order to more clearly illustrate the push-pull effect of **YH7**. *Opp*-dibenzoporphyrins **YH4** and **YH5** were prepared for comparison purposes. Porphyrins with similar structure have been evaluated as sensitizers for DSSCs in our previous work.[13] The novelty of this work is the utilization of a much bulkier porphyrin. Dye aggregation has long proven to be a severe problem, which leads to lower effective conversion of solar energy to electricity in DSSCs. The utilization of a bulky porphyrin is expected to lessen dye aggregation on the TiO_2 surface, which would minimize the need for co-adsorbents used to reduce dye aggregation.

The synthesis of benzoporphyrin **YH4** started from free-base dibromoporphyrin **1** (Scheme 1).[11a] The Heck reaction of **1** with methyl 2,4-pentadienoate followed by 6π-electrocyclization and aromatization[14] led to the formation of free-base monobenzoporphyrin **2** bearing acrylic esters in good yield. Zinc insertion and subsequent hydrolysis of the ester groups yielded **YH4**. Further bromination of **2** with NBS in refluxing 1,2-dichloroethane generated dibromobenzoporphyrin **3**. Dibromobenzoporphyrin **3** reacted with *p*-methoxystyrene through the Heck, 6π-electrocyclization, and aromatization sequence, which produced *opp*-dibenzoporphyrin **4**. Zinc insertion and subsequent hydrolysis of the ester groups yielded **YH5**.

Reaction of dibromobenzoporphyrin **3** with the corresponding enynes in the presence of Pd(0) catalyst through the Heck-based sequence reaction[14] produced *opp*-dibenzoporphyrin **5** and **6**. It is worth mentioning that different conditions are required with different alkenes for the Heck-based sequence reaction. For example, the reactions of methyl 2,4-pentadienoate and *p*-methoxystyrene with dibromoporphyrins **1** and **3,** respectively, were divided into two steps: first step, a bicatalytic system, i.e., $Pd[P(t\text{-}Bu)_3]_2/Pd_2(dba)_3$, was used in the Heck reaction at a lower temperature (45 °C) in THF generating the direct Heck products; second step, *p*-chloranil was used as the oxidant to facilitate the 6π-electrocyclization and subsequent aromatization to yield **2** and **4**, respectively. In contrast, the reaction of **3** with enynes were carried out in one-pot in the presence of $Pd[P(t\text{-}Bu)_3]_2$. In addition, no oxidant was added to these reactions. As demonstrated by the much lower yields, the reactions of bromoporphyrin **3** with enynes have turned out to be more difficult than with regular alkenes. This is likely due to the more severe polymerization reaction of enynes and the side reaction

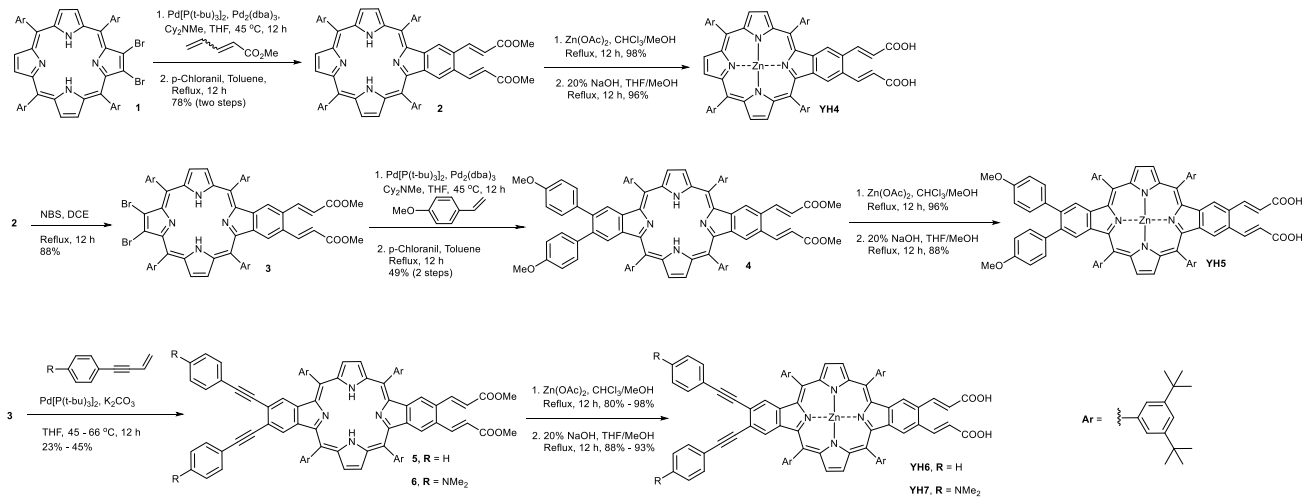

Scheme 1 Synthesis of benzoporphyrins **YH4**, **YH5**, and push-pull *opp*-dibenzoporphyrins **YH6**, **YH7** bearing phenylethynyl bridge

of enyne in the presence of Pd(0).[15] Zinc insertion then took place with **5** and **6**, followed by hydrolysis to furnish the final push-pull *opp*-dibenzoporphyrins **YH6** and **YH7**, respectively.

2.2 Optical properties

Normalized UV-Vis absorption spectra of dibenzoporphyrins **YH5-YH7** and monobenzoporphyrin **YH4** are compiled in Figure 3. While all the dibenzoporphyrins (**YH5**–**YH7**) display one intense Soret band and four Q bands, monobenzoporphyrin (**YH4**) displays one intense Soret band and only two Q bands, likely due to the symmetry change of the porphyrin core. The Soret band of monobenzoporphyrin **YH4** occurs at 455 nm. Upon fusion of one more benzene ring to the porphyrin periphery, the Soret is red-shifted by 15 nm to 470 nm in **YH5**. Introduction of the conjugated phenylethynyl bridge in **YH6** further red-shifted the Soret band by 5 nm to 475 nm. The Soret bands on these dibenzoporphyrins also contain a shoulder band. It is notable that the inclusion of the push (tertiary amine) groups in **YH7** further shifts the Soret band by 5 nm to 480 nm, and the shoulder of the Soret band is more discernible than that of **YH5** and **YH6**. These data suggest a better push-pull effect in **YH7** than in **YH5** and **YH6**. Although all dibenzoporphyrins (**YH5**–**YH7**) show four Q bands, the absorption patterns of **YH6** and **YH7** are clearly different from that of **YH5**. The Q bands of **YH7** are also slightly red-shifted relative to those of **YH6**.

Steady state fluorescence spectra of the three dibenzoporphyrins (**YH5**–**YH7**) exhibit a more intense emission band around 641 nm – 644 nm and a less intense emission band at 705 nm – 709 nm (Figure 3, inset). On the other hand, the intensity of the two emission bands in monobenzoporphyrin **YH4** is inversed, with the much more intense emission at 675 nm and much less intense emission at 615 nm. The fluorescence spectra onset of **YH4**–**YH7** roughly reflect a similar trend in their UV-Vis absorption spectra. The optical data of these porphyrins are organized in Table 1.

The fluorescence lifetime of **YH4**, measured using time correlated single photon counting (TCSPC) technique is found to be 2.14 ns. Similarly, the fluorescence lifetimes for **YH5**, **YH6**, and **YH7** are 1.01, 1.12, and 1.06 ns, respectively. The lifetimes of **YH5**–**YH7** are much shorter than that of **YH4**, indicating a

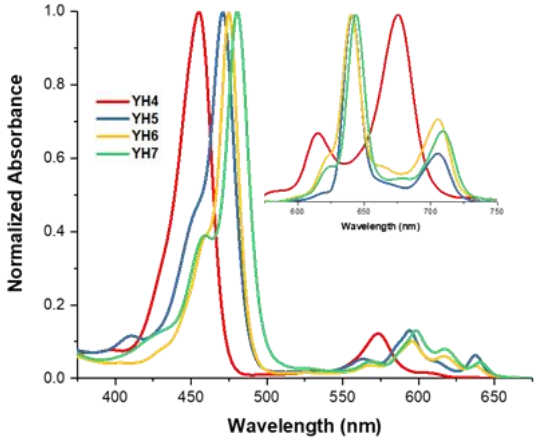

Figure 3 Normalized UV-Vis absorption spectra of **YH4**-**YH7** in THF. Inset: Normalized fluorescence spectra of **YH4**-**YH7** in THF. The compounds were excited at the most intense visible band maxima

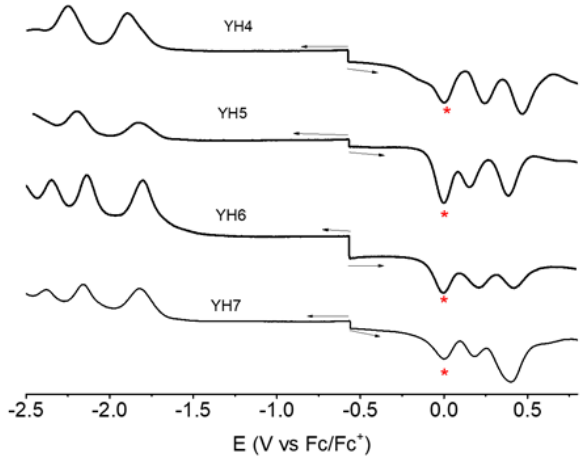

Figure 4 Differential pulse voltammograms (DPVs) of the investigated compounds in *o*-DCB containing 0.1 M (TBA)ClO_4. Ferrocene/ferrocenium redox couple was used as an internal standard

Table 1 Absorption, fluorescence, ground and excited state oxidation potentials of the investigated porphyrins, and the free-energy change for charge injection and recombination involving the porphyrins and TiO_2

Dye	$\lambda_{max}^{abs\,[a]}$ [nm] (ε, 10^5 M^{-1} cm^{-1})	$\lambda_{max}^{em\,[a]}$ [nm]	$E_{0\text{-}0}$ [b] [eV]	E_{ox} [c] [V]	E_{ox}^{*} [d] [V]	ΔG_{inj} [e] [eV]	ΔG_{reg} [f] [eV]
YH4	455 (3.40)	615, 675	2.10	1.04	-1.07	-0.57	-0.62
YH5	470 (3.27)	641, 705	1.94	0.94	-1.00	-0.50	-0.52
YH6	475 (4.58)	640, 705	1.94	0.99	-0.95	-0.45	-0.57
YH7	480 (2.11)	644, 709	1.93	0.99	-0.94	-0.44	-0.57

[a] Wavelength of the absorption and emission maxima in THF; The extinction coefficients (ε, 10^5 M^{-1} cm^{-1}) are shown in parentheses. [b] $E_{0\text{-}0}$ was determined from the intersection of normalized absorption and emission spectra. [c] The oxidation potentials of dyes were measured in *o*-DCB with 0.1 M (TBA)ClO_4 with a scan rate of 100 mVs^{-1}; Potentials measured vs. the Ag/AgCl (Ag/Ag^+) couple were converted to potentials vs. SHE. [d] Excited-state oxidation potentials (E_{ox}^{*}) was approximated from E_{ox} and $E_{0\text{-}0}$. [e] Driving force for electron injection (ΔG_{inj}) calculated from the energy difference between the dye excited singlet state (E_{ox}^{*}) and conduction band of TiO_2 (-0.5 V vs. SHE). [f] Driving force for regeneration (ΔG_{reg}) calculated from the energy difference between the porphyrin radical cation (E_{ox}) and the iodine (I^-/I_3^-) couple (+0.42 V vs. SHE).

push-pull effect may be at play in these porphyrins. It is interesting to note that the lifetime of **YH7**, which bears strong electron-donating amine groups, is only slightly shorter than that of **YH6**, which does not have electron-donating groups.

2.3 Electrochemical and spectroelectrochemical characterization

The electrochemical properties of these porphyrins were measured by cyclic and differential pulse voltammetric techniques in *o*-dichlorobenzene containing 0.1 M (TBA)ClO_4 as the supporting electrolyte. The electrochemical data is summarized in Table 1 and Table S2. Both monobenzoporphyrin **YH4** and dibenzoporphyrin **YH5** revealed two one-electron oxidations and two one-electron reductions (see Figure 4 for DPVs and Figure S2 for CV curves), which are typical of zinc porphyrin derivatives. On the other hand, both the dibenzoporphyrins **YH6** and **YH7** bearing the phenylethynyl bridge showed three one-electron reductions and two one-electron oxidations. Both the oxidation and the reduction processes were found to be reversible for **YH4** and **YH5**. The oxidation occurred at 0.25 and 0.49 V vs. Fc/Fc^+ for **YH4**. Upon fusion of one more benzene ring to the porphyrin periphery, both the first and the second oxidation potentials of **YH5** shifted more negative by 0.10 V and 0.11 V, respectively. On the other hand, inclusion of the phenylethynyl bridge in **YH6** moves the first and second oxidation potentials to 0.21 V and 0.41 V, respectively, more positive relative to those of **YH5**. The installation of strong electron-donating amine groups in **YH7** did not affect the oxidations significantly; only a slight negative shift by < 0.02V was observed. The two reduction processes were found at -1.91 V and -2.23 V vs. Fc/Fc^+ for **YH4**. The first two reductions of all the dibenzoporphyrins (**YH5**–**YH7**) shifted to more positive as compared with those of monobenzoporphyrin **YH4**. While the two reductions of **YH6** shifted to more positive relative to those of **YH5**, those of **YH7** shifted to more negative as compared to those of **YH6**. In addition, the push groups have a greater impact on the third reduction potential of **YH7** than on the first and second. The electrochemical HOMO–LUMO energy gap followed the order of **YH4** > **YH7** ~ **YH6** > **YH5**.

As part of complete characterization of the newly synthesized compounds, spectroelectrochemical studies were performed to characterize the one-electron oxidized and one-electron reduced products. Figure S3 in SI shows the spectra of the radical cation and radical anion of each zinc porphyrin. **YH4** with only one fused benzene ring revealed radical cation peaks at 455, 573, and 694 nm while the radical anion showed peaks at 435, 461, and 585 nm. For **YH5**–**YH7**, because of the presence of two fused benzene rings which extended the π-conjugation even further, the radical cation displayed broad near-IR peaks (overlap of two peaks centred around 730 and 790 nm) spanning the 650 – 800 nm range, in addition to new peaks in the visible range. Similarly, the radical anion also displayed new peaks in the visible region (see Figure S3). However, no peaks for the radical anion beyond 700 nm was observed.

The driving force for dye regeneration (ΔG_{reg}) of oxidized dyes from the electron mediator (I^-/I_3^-) was estimated based on the experimental first oxidation potentials of **YH4**–**YH7**. All of these dyes possess first oxidation potentials > 0.5 V, more positive than the potential of the redox mediator I^-/I_3^- (0.42 V vs SHE), indicating thermodynamically feasible regeneration of oxidized dye from electron mediator.

The driving force for electron injection (ΔG_{inj}) from the excited dye to the conduction band of the semiconductor was also estimated. Such optical and electrochemical data are compiled in Table 1. The calculated excited state oxidation potentials (E_{ox}^{*}) for **YH4**-**YH7** are -1.07 V, -1.00 V, -0.95 V, and -0.94 V, respectively. The LUMO energy levels of **YH4** and **YH5** are sufficiently higher than that of the conduction band for TiO_2 (-0.50 V vs SHE) to ensure efficient electron injection from the photo-excited porphyrin dyes to the conduction band of the TiO_2 (Figure 5). In contrast, the LUMO energy levels of **YH6** and

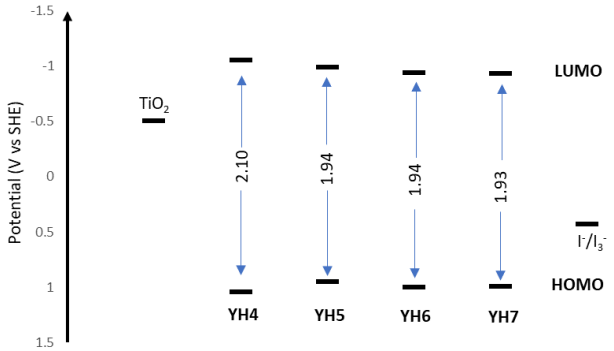

Figure 5 Energy level diagram of HOMO and LUMO of **YH4**, **YH5**, **YH6** and **YH7**

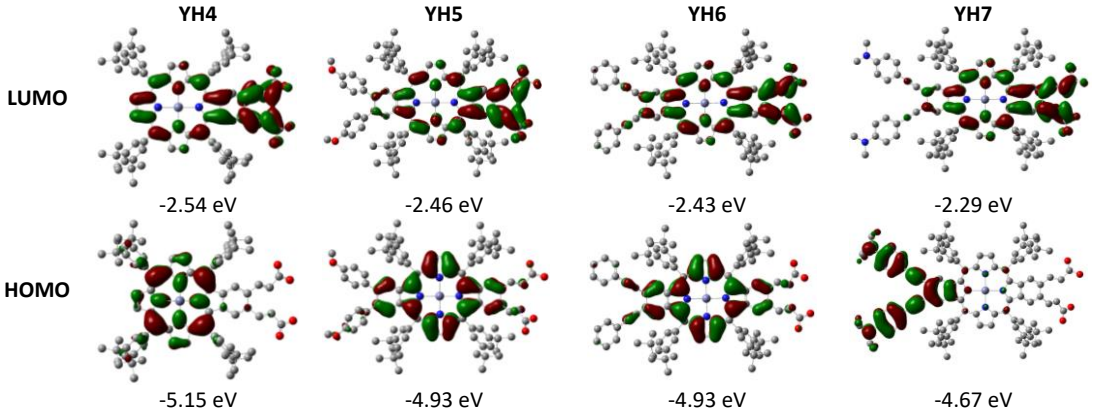

Figure 6 Isodensity surface of the HOMO and LUMO for **YH4**–**YH7** calculated by Gaussian09 DFT B3LYP/6-31G(d,p)

YH7 lie slightly lower than the energy level expected for thermodynamically feasible electron injection. The HOMO–LUMO energy gap calculated from UV-Vis and emission spectra is in the order of **YH4** > **YH5** = **YH6** > **YH7**, which differ from their electrochemical HOMO–LUMO energy gap. However, it is important to note that overall HOMO–LUMO gap for the mono-benzo fused porphyrin (**YH4**) is higher than the bis-benzo fused porphyrins (**YH5**–**YH7**), from both spectral and electrochemical studies.

2.4 DFT calculations

In order to better understand the orbital coefficients on the frontier molecular orbitals, DFT calculations (*Gaussian 09* DFT B3LYP/6-31G(d,p)) were conducted for **YH4**–**YH7**. The calculated geometries of these molecules are included in the Supporting Information (Figure S4). The optimized structure reveals a roughly planar geometry for **YH4**. Upon fusion of one more benzene ring to the porphyrin periphery at the opposite side, all the dibenzoporphyrins (**YH5**–**YH7**) become distorted from planarity. The distortion is more severe in **YH5** compared with **YH6** and **YH7**. Similar to **YH3**[13] the aryl groups at the 12^2 and 12^3 positions of **YH5** did not lie in the same plane with the porphyrin core, which hinders the electronic communication between them. In contrast, the arylethynyl groups of **YH6** and **YH7** stayed in the same plane with the porphyrin core, which is expected to facilitate intramolecular electronic communication.

The LUMO of these porphyrin dyes was mainly located at the porphyrin core and extended into the fused benzene ring bearing the acrylic acid anchoring groups (Figure 6). Slightly increased participation of the opposite fused benzene ring is visible for **YH6** and **YH7**. The heavy involvement of the anchoring group in the LUMO is expected to facilitate the electron injection from the photoexcited dye to the conduction band of TiO_2 due to increased electronic coupling between the excited state of the dye and the 3d orbitals of TiO_2.[5g,16]

The HOMO of the monobenzoporphyrin **YH4** predominately occupied the porphyrin core without the participation of the fused benzene ring. On the other hand, the HOMO of dibenzoporphyrins **YH5** and **YH6** involved both the porphyrin core and the two fused benzene rings, with slight participation of the ethynyl bridge in **YH6**. In sharp contrast, the HOMO of **YH7** displays a completely different feature. The HOMO of **YH7** is mainly located at the donor (tertiary amine) groups, the phenylethynyl bridges and the fused benzene ring to which the phenylethynyl bridges are attached. The porphyrin core is not involved. It should be mentioned that the energy levels of HOMO and HOMO-1 for **YH7** are very close with only 0.02 eV difference. The HOMO-1 of **YH7**, on the other hand, engages the phenylethynyl bridges and the donor groups with inclusion of the porphyrin core (see Figure S4). The characteristics of the HOMOs and LUMOs demonstrate significant orbital segregation, which is a much-favoured feature for DSSCs. Considering the only structural difference between **YH6** and **YH7** is that **YH7** bears electron-donating 3° amine groups and **YH6** does not, the impact on HOMO brought by the 3° amine groups is immense. The order of the calculated HOMO-LUMO energy gap is **YH4** (2.61 eV) > **YH6** (2.50 eV) ~ **YH5** (2.47 eV) > **YH7** (2.38 eV). This order roughly agrees with that of the optical energy gap, but not with that of the electrochemical energy gap. The discrepancy could be attributed to solvent effects as optical and electrochemical experiments were conducted in different solvents.

2.5 Evidence of charge injection – Femtosecond Transient Absorption studies

Femtosecond transient absorption spectral studies were performed to characterize the push-pull porphyrins in solution and immobilized on a transparent TiO_2 surface. The presence of electron rich and poor substituents on the opposite end of the porphyrin π-ring could promote intramolecular type charge transfer within the molecules. Under such circumstances, the transient spectral features would reveal new peaks corresponding to the charge transfer state. This is in addition to the transient spectral features for what could be expected for the simple zinc porphyrins without any push-pull effects. Such charge transfer could also result in faster deactivation of the singlet excited state. Figure 7 shows the transient spectra at the indicated delay times of **YH4**–**YH7** in MeOH/$CHCl_3$ (v/v = 4/1) at an excitation wavelength corresponding to either porphyrin Q-band or Soret band. This solvent mixture was selected for better solubility of the investigated compounds. In the case of **YH4**, the instantly formed ^{1}**YH4*** (see the spectrum at 2 ps) revealed

transient peaks at 494 and 648 nm and negative peaks at 580 nm, due to ground state bleaching, and at 684 nm corresponding to stimulated emission. The decay of positive peaks and recovery of negative peaks were slow, consistent with the earlier discussed average lifetime of 2.14 ns. Interestingly, for **YH5**–**YH7** distinct spectral features supporting intramolecular type charge transfer due to push-pull effect were observed. In all of these compounds, the instantly formed singlet excited state revealed broad peaks in the 525 – 575 nm range, and peaks at 635 and 665 nm range. Negative peaks in the 570, 595, 640, and 710 nm range were also observed. By comparison with the earlier discussed UV-Vis and fluorescence studies, the first two negative peaks were assigned to ground state bleaching while the latter two negative peaks to stimulated emission. Importantly, new peaks in the 735 and 790 nm range were also observed while the positive spectral features in the 600 – 700 nm range were much more intense than that observed for **YH4**. Please note that the 790 nm peaks were noisy due to the detection limit of our detector. The spectroelectrochemical data discussed earlier revealed peaks in the 600 – 700 nm range for the radical anion and in the near-IR (650 – 800 nm) range corresponding to the radical cation for **YH5**–**YH7**. Data shown here indeed revealed the existence of transient signals which correspond to both radical anion and radical cation in the case of **YH5**–**YH7**, which support intramolecular charge transfer within the push-pull system. In addition, as supported by the lifetime studies, the decay/recovery of the peaks was rather rapid, which populated the triplet excited state of each system. In the case of **YH7**, some photodecomposition of the porphyrin was also observed.

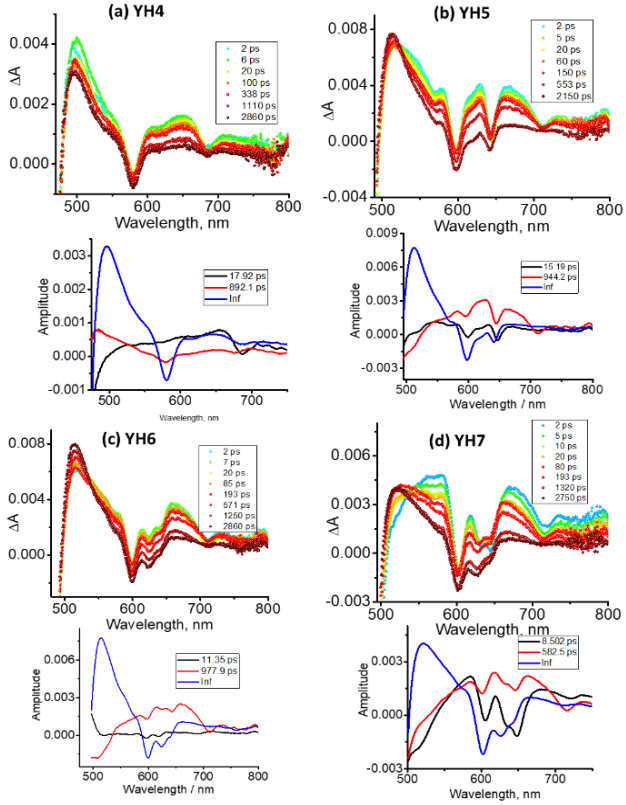

Figure 7 Femtosecond transient absorption spectra at the indicated delay times of the push-pull porphyrins in MeOH/$CHCl_3$ (v/v = 4/1). Excitation wavelength of 547 nm for **YH4**, 479 nm for **YH5**, 474 nm for **YH6**, and 485 nm for **YH7** were used. The lower panel shows decay associated spectra constructed to extract the kinetic information of photoevents.

The transient data was analysed by constructing decay associated spectra (DAS) for each system, as shown in the lower panels of Figure 7. Such analysis yielded three components for each system. By analogy with the lifetime data and spectral features, in the case of **YH4**, the first component with a lifetime of 17.9 ps was assigned to formation of **^{1}YH4*,** second one with a time constant of 892.1 ps for the decay of **^{1}YH4*** and the third one with a time constant beyond 3 ns to **^{3}YH4***, an intersystem crossing product. In the case of **YH5**-**YH7**, the first DAS revealing negative amplitude (rise component) at positions where both cation and anion radical signals are expected are within few picoseconds, suggesting formation of charge transfer state at this time scale. The second component with positive amplitude (decay component) at wavelengths corresponding to the charge transfer state is attributed to the lifetime of charge transfer state. The third component, whose lifetime was beyond 3 ns and has triplet excited state features of the push-pull porphyrins, was assigned as population of the triplet excited state. The observed time constants for the first two processes were found to be 15.2, 11.4, and 8.99 ps, and 944.2, 934.3, and 582.5 ps, respectively, for **YH5**, **YH6**, and **YH7**.

Figure 8 shows transient and DAS for **YH4**–**YH7** anchored on transparent semiconducting TiO_2 surface. Here, films of transparent TiO_2 of 6 μM thickness developed using the Doctor-Blade technique were employed. The selected porphyrin in a MeOH/$CHCl_3$ solvent mixture was allowed to surface adsorb (1-2 h) onto TiO_2, then the films were rinsed thoroughly using $CHCl_3$ to remove unbound porphyrin. For data collection, using a solid film mount, the sample was moved slowly to avoid photodecomposition. Thermodynamic feasibility of charge injection from excited porphyrin to the conduction band of TiO_2 is discussed earlier with the help of Figure 5. In all of the systems, viz., **YH4**/TiO_2 to **YH7**/TiO_2, charge injection was predicted. The spectral data shown in Figure 8 indicate this indeed to be true. In all of the **YH4**/TiO_2 to **YH7**/TiO_2 systems, transient features corresponding to radical cation of porphyrin at the expected wavelengths was possible to observe. In addition, the photochemical events were rather rapid compared to what was observed in solution for a given porphyrin. For **YH4** – **YH6,** signal relaxation was completed within 40-50 ps while that for **YH7** was close to 20 ps. For data analysis, DAS were generated as shown in bottom panels of each figure. Such analysis yielded two main components. The first one with time constants of 1-2 ps while a second component with time constants of 6-20 ps, both revealing decay of the singlet excited state as a result of charge injection from the excited states to TiO_2. Multiple components suggest existence of multiple environments for porphyrin adsorbed on TiO_2. The second component was utilized to evaluate the average charge injection time constants which yielded 19.5 ps for **YH4**, 16.3 ps for **YH5**, 20.0 ps for **YH6** and 6.3 ps for **YH7**, respectively. Although faster charge injection was observed in the case of **YH7**, the sample revealed significant decomposition,

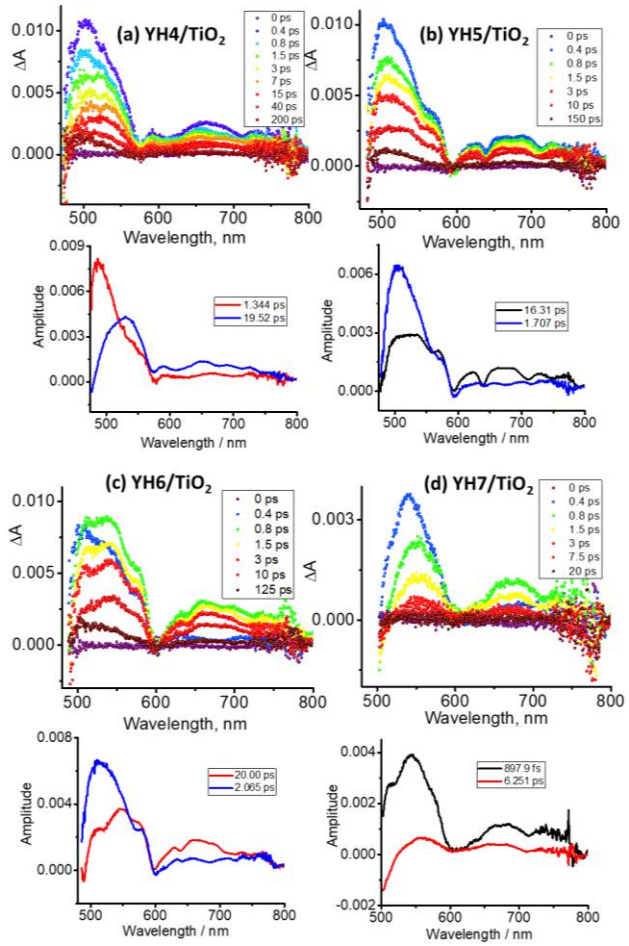

Figure 8 Femtosecond transient absorption spectra at the indicated delay times of the push-pull porphyrins decorated on transparent TiO_2. Excitation wavelength of 547 nm for **YH4**, 479 nm for **YH5**, 474 nm for **YH6**, and 485 nm for **YH7** were used. The lower panel shows decay associated spectra constructed to extract the kinetic information of photoevents.

hence, the time constants could be viewed as lower limit. A much weaker third component with time constants of few ns was also observed (data not shown) that could be attributed to charge recombination process. Earlier, time scales of this order for charge recombination were reported by Imahori and Sundstrom groups for *meso*-functionalized zinc porphyrin immobilized on TiO_2 systems.[20] In general, faster charge injection was witnessed with increased push-pull effect of the current porphyrin series, i.e., **YH7** > **YH5** > **YH6** > **YH4**.

2.6 Photovoltaic performance

Photocurrent-voltage (*J-V*) curves and IPCE action spectra were used to evaluate the photovoltaic performance of the DSSCs sensitized with **YH4**–**YH7**. Both *J-V* curves and IPCE spectra were measured under simulated AM 1.5 one sun (100 mW cm^{-2}) illumination on cells with a 0.16 cm^2 active area. The light to power conversion efficiency (η) was determined based on equation (1), where J_{SC} is short-circuit current density, V_{OC} is open circuit voltage, and FF is fill factor.

$$\eta = J_{SC} \times V_{OC} \times FF \qquad (1)$$

The calculated values for the best of three cells are listed in Table 2 while η values are average of these three cells.

2.6.1 Dye adsorption time

First, we investigated optimum dye soaking time for dye adsorption onto TiO_2 surface in order to maximize the performance, and used **YH4** as the reference dye. As shown in Table S3, variable values were obtained for the overall power conversion efficiency (PCE) and photocurrent density of the dye with variable dye soaking time. The PCE value of **YH4** increased with increased soaking time and reached the highest in 3 h, then decreased with further increased soaking time. It is noticeable that the increase in J_{SC} value mainly accounted for the initial increase in efficiency. With longer soaking time (> 3 h) the efficiency decreased with decreased values of both V_{OC} and J_{SC}. It appears that the initial rise in the J_{SC} values with elongated dye soaking time is likely the outcome of increased dye loading onto the photoanode. However, when the dye adsorption time was too long, dye molecules start to aggregate on the photoanode, leading to lower J_{SC} and V_{OC} values.

2.6.2 Dye aggregation effect

Dye aggregation is generally believed to have an adverse effect on carrier photogeneration through self-quenching of the excited state. Chenodeoxycholic acid (CDCA) is known to minimize dye aggregation via co-adsorption with the dye onto the TiO_2 surface. It is expected that the addition of CDCA would help to improve both V_{OC} and J_{SC} values through reduction of the dye aggregation on TiO_2. We then investigated the effect of CDCA through sensitizing **YH4** with different concentrations of CDCA (0 mM– 1.0 mM CDCA) (see SI Table S4). The best PCE value was achieved when 0.6 mM CDCA was used as a co-absorbent with **YH4**. This CDCA concentration also worked well

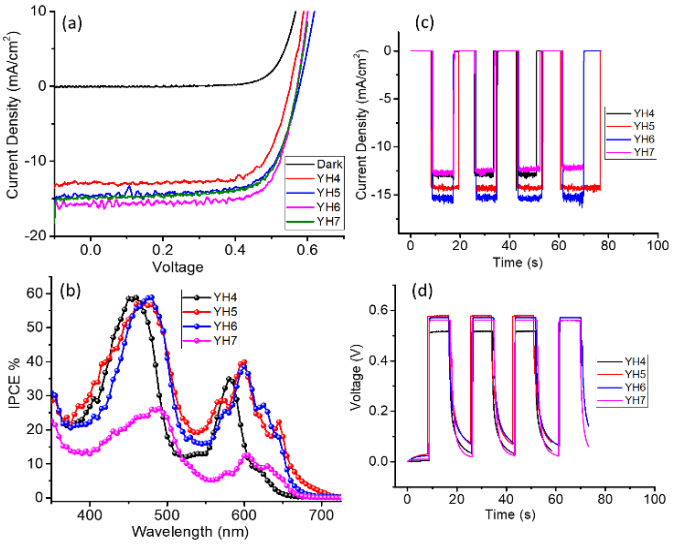

Figure 9 (a) *J-V* plots, (b) IPCE curves, (c) current switching and (d) potential switching of DSSCs developed in the present study

Table 2 Photovoltaic performance of DSSCs based on **YH4**, **YH5**, **YH6** and **YH7**

Dye	J_{SC} (mA/cm^2)	V_{OC} (V)	FF	η (%) [d]
YH4[a]	13.12	0.55	0.68	4.91[e] (4.86 ± 0.08)
YH5[a]	14.81	0.58	0.65	5.56[e] (5.52 ± 0.04)
YH6[b]	16.12	0.58	0.72	6.70[e] (6.57 ± 0.09)
YH7[c]	15.12	0.57	0.66	5.72[e] (5.04 ± 0.50)

The photovoltaic measurements were conducted under AM 1.5G illumination (power 100 mW cm^{-2}) in the presence of a mask and with a cell active area of 0.16 cm^2 and a TiO_2 thickness of 25 µm. As a reference, efficiency of N719-sensitized solar cells was determined: J_{SC} = 16.5 mA cm^{-2}, V_{OC} = 0.67 V, FF = 0.63, and η = 7.4%. [a] The TiO_2 film was soaked in 0.3 mM dye solution in MeOH/$CHCl_3$ (v/v = 3/1) containing 0.6 mM CDCA for 3 h. [b] The TiO_2 film was soaked in 0.2 mM dye solution in MeOH/$CHCl_3$ (v/v = 2/1) without CDCA for 3 h. [c] The TiO_2 film was soaked in 0.2 mM dye solution in MeOH/$CHCl_3$ (v/v = 1/1) without CDCA for 3 h. [d] The average for PCE of each dye obtained from 3 devices are given in parentheses and ± refers to the standard deviation. [e] Best device PCE

with **YH5**. However, it turns out that the best PCEs were obtained for **YH6** and **YH7** cells in the absence of CDCA.

2.6.3 Power conversion efficiency

The photovoltaic performance of **YH4**–**YH7** is shown in Figure 9 and the data are summarized in Table 2. The power conversion efficiency (PCE, η) of the **YH4**-sensitized solar cell is 4.9%. Upon fusion of one more benzene ring, the PCE of **YH5**-sensitized solar cells increased to 5.6%. The increased PCE value of **YH5** can be attributed to its greater J_{SC} value. As shown in the UV-vis spectra (Figure 3), **YH5** displayed largely red-shifted Soret and Q bands as compared with **YH4**. The Q bands are also broadened compared to those of **YH4**, which suggests **YH5** is likely to have better light harvesting efficiency (LHE). The increased J_{SC} is also reflected on the IPCE spectra (Figure 9b, *vide infra*). **YH5**-sensitized solar cells exhibited higher IPCE values at the various Q-band regions as compared to the cell sensitized with **YH4**. These data are consistent with the PCEs reported previously for benzoporphyrins with similar structures.[11a]

YH6-sensitized solar cells achieved even higher PCE (η = 6.7%) than the solar cells based on **YH5**. The J_{SC} value of **YH6** sensitized solar cells reached 16.12 mA/cm^2, which is higher than those of **YH4** and **YH5**-sensitized solar cells, suggesting inclusion of a phenylethynyl bridge largely enhanced the light harvesting efficiency (LHE). On the other hand, the V_{OC} values of the **YH4**-, **YH5**-, and **YH6**-sensitized solar cells are almost similar, indicating these three solar cells have similar kinetic processes for electron injection and charge collection (TiO_2), a trend that agrees well with the earlier discussed femtosecond transient spectral data where ultrafast charge injection was witnessed. **YH4**, **YH5**, and **YH6** carry exactly the same anchoring groups (acrylic acids), and as such, the charge collection efficiencies (η_{col}) of these solar cells which is a result of competition between charge recombination and collection, are likely to be similar.[17] Based on the electron injection data, the electron injection rates for **YH4**, **YH5**, and **YH6** are also similar, indicating push-pull effect are almost the same in **YH5** and **YH6**.

Significant decomposition was observed for **YH7** on TiO_2 surface. The dark green-coloured surface of the **YH7**-sensitized device became pale coloured after irradiation. Despite the decomposition, we were able to evaluate the photovoltaic performance of **YH7**-sensitized solar cells. A PCE up to 5.7% was obtained under optimized conditions. Although the PCE is lower than that of the **YH6**-sensitized solar cell, given the observed substantial degradation of **YH7** upon irradiation within 20 min, this PCE value is still high.

The current and potential switching plots shown in Figures 9c and d reveal quite reproducible results for **YH4**–**YH6**, which is indicative of their robustness. However, noticeable lowering of current during successive switching of **YH7** was observed due to photobleaching.

2.6.4 IPCE values

These dyes were adsorbed on TiO_2 surface using the optimal dye absorbing time (3 h) at optimal dye concentration in the presence of the co-absorbent CDCA. The incident photon-to-current efficiency (IPCE%) spectra measured for selected dye-sensitized devices (note - not the best performing cells shown in Figure 9a) are shown in Figure 9b. The IPCE% (λ) values were derived from equation (2), where LHE is the light harvesting efficiency, Φ_{inj} is the quantum yield of electron injection from the excited sensitizer into TiO_2, and η_{col} is the electron collection efficiency.

$$\text{IPCE}(\lambda) = \text{LHE} \times \Phi_{\text{inj}} \times \eta_{\text{col}} \qquad (2)$$

In general, the IPCE% spectra of **YH4**, **YH5**, and **YH6** display similar patterns with higher IPCE values (up to 60%) at the Soret band region and lower IPCE values (up to 40%) at the Q band

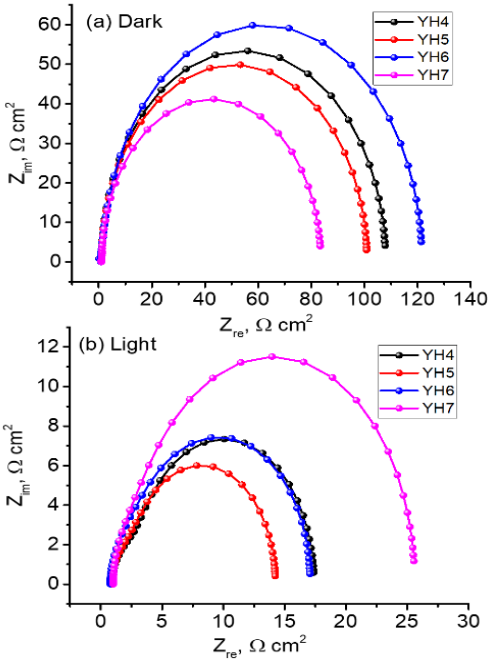

Figure 10 Nyquist plots for (a) FTO/TiO_2/ZnP (ZnP = **YH4**–**YH7**) measured at respective V_{OC} under (a) dark and (b) AM 1.5 filtered light illumination conditions

Table 3 Charge transfer resistance values of FTO/TiO_2/ZnP (ZnP = **YH4**–**YH7**) and counter Pt electrodes (at the respective VOC) estimated using electrochemical impedance spectroscopy

Dye	Conditions	R_{ct} (Ω cm^{-2})
YH4	Dark	106.9
	Light	14.4
YH5	Dark	99.9
	Light	11.7
YH6	Dark	119.8
	Light	14.4
YH7	Dark	82.6
	Light	22.5

region. These IPCE values are close to those of our previously reported benzoporphyrins.[13] Not surprisingly, the IPCE values of **YH7** are much lower than those of **YH4**–**YH6** due to degradation of **YH7** over long exposure of light.

2.6.5 Photodegradation investigation of YH7

We noticed that **YH7** does not decompose in dark, regardless of being in solution or in solid state under ambient conditions based on ^{1}H NMR, UV-vis absorption data, as well as TLC analysis. Our UV-vis spectroscopic data also indicate that **YH6** and **YH7** have similar stability on TiO_2 surface under ambient conditions (Figure S5). It is possible that **YH7** degrades only under irradiation. To prove this point, **YH6** and **YH7** were irradiated under AM 1.5 G illumination in MeOH/$CHCl_3$ solution, and the degradation was tracked with UV-vis spectroscopy. Surprisingly, **YH6** and **YH7** displayed similar level of stability (Figure S6). Solar cell stability studies reveal that PCE of **YH6** cell increased in 3 h and only slightly decreased after 20 h. In contrast, PCE of **YH7** cell continually decreased within the 20 h window. It appears that **YH7** degrades on TiO_2 surface upon illumination. It has been reported that the presence of triethanolamine (TEA) facilitates the photobleaching of porphyrins.[18] It is likely that the tertiary amino groups on **YH7** are the key factors causing this severe photodegradation. On the other hand, such photodegradation has not been reported for other porphyrins dyes carrying amino groups. The photodecomposition mechanism of **YH7** remains unclear, and is worthy of further investigation.

2.7 Electrochemical Impedance Spectroscopy (EIS) studies

EIS experiments were carried out to estimate interfacial charge transfer resistance in solar cells derived from **YH4**–**YH7**.[19] Figure 10 shows the Nyquist plots under dark and light conditions as two semicircles. The smaller semicircles in the high frequency range (left side of the plot) reflect the charge transfer at the counter electrode/electrolyte interface while the larger semicircles in the low frequency range (right side of the plot) correspond to the TiO_2/porphyrin/(I^-/I_3^-) electrolyte interface. The charge transfer resistance, obtained by building an equivalent circuit, of the counter electrode/electrolyte interface was found to be small under both light illumination and dark conditions (smaller radius for the semicircles). Interestingly, as revealed by the larger radius of the semi-circles, substantially lower R_{ct} were obtained for the TiO_2/ZnP/redox interface under light illumination conditions compared to the value gathered in dark conditions (Table 3). Generally, a smaller R_{ct} value for the TiO_2/dye/redox interface can be attributed to superior photo-regeneration ability which resulted in an increased light energy conversion efficiency.[21] From the data shown in Table 3, a comparatively lower value for TiO_2/**YH4**–**YH6**/redox interfaces were witnessed which agrees with higher performance of the DSSCs derived from these compounds. For the TiO_2/**YH7**/redox interface, the R_{ct} value was comparatively higher. It should be pointed out that the magnitude and trends in R_{ct} values obtained are comparable to those reported by us on other zinc porphyrin derived DSSCs, recorded under similar experimental conditions.[22]

3. Conclusions

A series of β-functionalized push-pull *opp*-dibenzoporphyrins (**YH4**–**YH7**) were designed, synthesized, and characterized by various physico-chemical techniques, and were then evaluated for their performance in dye-sensitized solar cells. This series of compounds were designed to systematically investigate the key structural factors in designing β-functional π-extended porphyrins as new generations of sensitizers for dye-sensitized solar cells. A remarkable push-pull effect was observed for **YH7**. In this case, incorporation of the phenylethynyl bridge has proved to be an effective strategy to allow enhanced interaction of the electron-donating group and the electron-accepting group within the molecule. The installation of the strongly electron-donating tertiary amine group is also critical to cause the pronounced push-pull effect in **YH7**. DFT orbital calculations revealed significant orbital segregation, a much sought-after feature for dyes used in DSSCs. Femtosecond transient absorption studies provided evidence of efficient charge injection from the singlet excited state of zinc porphyrin to the conduction band of TiO_2 for all studied porphyrin dyes (**YH4**–**YH7**). In particular, porphyrin **YH7**, bearing both the phenylethynyl bridge and the tertiary amine group, displayed much faster charge injection (6.3 ps) than **YH4**–**YH6** (16.3 – 20.0 ps) due to the push-pull effect.

The photovoltaic performances of these benzoporphyrins were quite remarkable. A monobenzoporphyrin **YH4** based solar cell gave PCE of 4.9%. Upon fusion of one more benzene ring, the PCE of the *opp*-dibenzoporphyrin **YH5** cell increased to 5.6%. Inclusion of the phenylethynyl bridge in **YH6** further enhanced the PCE to 6.7%. Despite its much favourable properties brought by the push-pull effect, **YH7** cells only achieved a PCE of 5.7%. The lower than expected PCE is attributed to the photoinduced degradation of **YH7** on TiO_2 surface. Nevertheless, the high PCE of **YH6** cell (6.7%), which is comparable to that of N719 cell (7.4%) under similar conditions, suggests great potential for these types of π-extended porphyrins. Investigation into structural factors causing and reducing the illumination-induced photodegradation of these types push-pull porphyrins are currently underway.

Conflicts of interest

There are no conflicts to declare.

Acknowledgements

This work was supported by the U.S. Department of Energy, Office of Science, Basic Energy Sciences under Award (DE-SC0016766). Our gratitude goes out to Dr. Guido Verbeck and the Laboratory for Imaging Mass Spectrometry at the University of North Texas for MALDI-Orbitrap Mass Spectrometry data. We thank Dr. Yiming Cao and Dr. Michael Grätzel for obtaining some preliminary DSSC data.

Notes and references

1 a) A. Hagfeldt, G. Boschloo, L. Sun, L. Kloo and H. Pettersson, *Chem. Rev*., 2010, **110**, 6595-6663; b) B. O'Regan and M. Grätzel, *Nature*, 1991, **353**, 737-740; c) L. M. Gonçalves, V. de Zea Bermudez, H. A. Ribeiro and A. M. Mendes, *Energy Environ. Sci*, 2008, **1**, 655; d) A. Kay and M. Graẗzel, *J. Phys. Chem*., 1993, **97**, 6272-6277; e) A. Reynal and E. Palomares, Eur. J. *Inorg. Chem*., 2011, **2011**, 4509-4526; f) L. Zayat, O. Filevich, L. M. Baraldo and R. Etchenique, *Philos Trans A Math Phys Eng Sci*., 2013, **371**, 20120330.

2 a) W. M. Campbell, K. W. Jolley, P. Wagner, K. Wagner, P. J. Walsh, K. C. Gordon, L. Schmidt-Mende, M. K. Nazeeruddin, Q. Wang, M. Graẗzel, D. L. Officer, *J. Phys. Chem. C*, 2007, **111**, 11760-11762; b) H. Imahori, T. Umeyama, S. Ito, *Acc. Chem. Res.*, 2009, **42**, 1809-1818; c) R. Argazzi, N. Y. Murakami Iha, H. Zabri, F. Odobel, C. A. Bignozzi, *Coord. Chem. Rev.,* 2004, **248**, 1299-1316.

3 a) C. W. Lee, H. P. Lu, C. M. Lan, Y. L. Huang, Y. R. Liang, W. N. Yen, Y. C. Liu, Y. S. Lin, E. W. G. Diau and C. Y. Yeh, *Chem. Eur. J.,* 2009, **15**, 1403-1412; b) C. F. Lo, L. Luo, H. P. Lu, C. S. Hung and E. W. G. Diau, *J. Phys. Chem. C,* 2009, **113**, 755-764.

4 I. Obraztsov, W. Kutner and F. D'Souza, *Solar RRL*, 2017, **1**, 1600002.

5 a) S. Mathew, A. Yella, P. Gao, R. Humphry-Baker, B. F. Curchod, N. Ashari-Astani, I. Tavernelli, U. Rothlisberger, M. K. Nazeeruddin and M. Gratzel, *Nat. Chem*., 2014, **6**, 242-247; b) J. P. Hill, Angew. *Chem. Int. Ed. Engl*., 2016, **55**, 2976-2978; c) C.-L. Wang, J.-Y. Hu, C.-H. Wu, H.-H. Kuo, Y.-C. Chang, Z.-J. Lan, H.-P. Wu, E. Wei-Guang Diau and C.-Y. Lin, *Energy Environ. Sci*., 2014, **7**, 1392; d) A. Yella, H.-W. Lee, H. N. Tsao, C. Yi, A. K. Chandiran, M. K. Nazeeruddin, E. W.-G. Diau, C.-Y. Yeh, S. M. Zakeeruddin and M. Grätzel, *Science*, 2011, **334**, 629-634; e) A. Yella, C. L. Mai, S. M. Zakeeruddin, S. N. Chang, C. H. Hsieh, C. Y. Yeh and M. Gratzel, Angew. *Chem. Int. Ed. Engl*., 2014, **53**, 2973-2977; f) T. Bessho, S. M. Zakeeruddin, C. Y. Yeh, E. W. Diau and M. Gratzel, *Angew. Chem. Int. Ed. Engl*., 2010, **49**, 6646-6649; g) C.-W. Lee, H.-P. Lu, C.-M. Lan, Y.-L. Huang, Y.-R. Liang, W.-N. Yen, Y.-C. Liu, Y.-S. Lin, E. W.-G. Diau and C.-Y. Yeh, *Chem. Eur. J*., 2009, **15**, 1403-1412; h) J.-M. Ji, H. Zhou and H. K. Kim, *J. Mater. Chem. A*, 2018, **6**, 14518-14545; i) H. Meier, Z.-S. Huang and D. Cao, *J. Mater. Chem. C*, 2017, **5**, 9828-9837; j) A. Mahmood, J.-Y. Hu, B. Xiao, A. Tang, X. Wang and E. Zhou, *J. Mater. Chem. A*, 2018, **6**, 16769-16797; k) M. Urbani, M.-E. Ragoussi, M. K. Nazeeruddin and T. Torres, *Coord. Chem. Rev.,* 2019, **381**, 1-64; l) G. Di Carlo, A. O. Biroli, F. Tessore, S. Caramori and M. Pizzotti, *Coord. Chem. Rev.,* 2018, **358**, 153-177.

6 a) Y. Wu, W. H. Zhu, S. M. Zakeeruddin and M. Gratzel, *ACS Appl. Mater Interfaces*, 2015, **7**, 9307-9318; b) T. Higashino and H. Imahori, *Dalton Trans*., 2015, **44**, 448-463; c) B. J. Brennan, M. J. Llansola Portoles, P. A. Liddell, T. A. Moore, A. L. Moore and D. Gust, *Phys. Chem. Chem. Phys*., 2013, **15**, 16605-16614; d) T. Higashino, Y. Kurumisawa, H. Iijama, and H. Imahori, *Chem. Eur. J*. 2019, **25**, 538-547.

7 G. Di Carlo, A. O. Biroli, F. Tessore, S. Caramori and M. Pizzotti, *Coord. Chem. Rev*., 2018, **358**, 153-177.

8 a) H. Hayashi, A. S. Touchy, Y. Kinjo, K. Kurotobi, Y. Toude, S. Ito, H. Saarenpaa, N. V. Tkachenko, H. Lemmetyinen and H. Imahori, *ChemSusChem*, 2013, **6**, 508-517; b) H. Imahori, H. Iijima, H. Hayashi, Y. Toude, T. Umeyama, Y. Matano and S. Ito, *ChemSusChem*, 2011, **4**, 797-805; c) A. Kira, Y. Matsubara, H. Iijima, T. Umeyama, Y. Matano, S. Ito, M. Niemi, N. V. Tkachenko, H. Lemmetyinen and H. Imahori, *J. Phys. Chem. C*, 2010, **114**, 11293-11304; d) R. Deshpande, B. Wang, L. Dai, L. Jiang, C. S. Hartley, S. Zou, H. Wang and L. Kerr, *Chem, Asian, J*., 2012, **7**, 2662-2669; e) F. Lodermeyer, R. D. Costa, J. Malig, N. Jux and D. M. Guldi, *Chem. Eur. J*, 2016, **22**, 7851-7855; f) G. Zanotti, N. Angelini, G. Mattioli, A. M. Paoletti, G. Pennesi, G. Rossi, D. Caschera, L. d. Marcoc and G. Giglide, *RSC Adv*., 2016, **6**, 5123 - 5133; g) M. Ishida, S. W. Park, D. Hwang, Y. B. Koo, J. L. Sessler, D. Y. Kim and D. Kim, *J. Phys. Chem. C*, 2011, **115**, 19343–19354; h) F. Lu, Y. Feng, X. Wang, Y. Zhao, G. Yang, J. Zhang, B. Zhang and Z. Zhao, *Dyes Pigm*., 2017, **139**, 255-263.

9 a) M. Ishida, D. Hwang, Y. B. Koo, J. Sung, D. Y. Kim, J. L. Sessler and D. Kim, *Chem. Commun*., 2013, **49**, 9164-9166; b) M. Ishida, D. Hwang, Z. Zhang, Y. J. Choi, J. Oh, V. M. Lynch, D. Y. Kim, J. L. Sessler and D. Kim, *ChemSusChem*, 2015, **8**, 2967-2977; c) M. Ishida, S. W. Park, D. Hwang, Y. B. Koo, J. L. Sessler, D. Y. Kim and D. Kim, J. *Phys. Chem. C*, 2011, **115**, 19343-19354.

10 a) T. D. Lash, *J. Porphyrins Phthalocyanines*, 2001, **5**, 267-288; b) C. M. Carvalho, T. J. Brocksom and K. T. de Oliveira, *Chem. Soc. Rev*., 2013, **42**, 3302-3317; c) A. V. Cheprakov and M. A. Filatov, *J. Porphyrins Phthalocyanines*, 2009, **13**, 291-303.

11 a) R. G. Jinadasa, B. Li, B. Schmitz, S. Kumar, Y. Hu, L. Kerr and H. Wang, *ChemSusChem*, 2016, **9**, 2239-2249; b) B. Schmitz, B. Li, R. G. Waruna Jinadasa, S. B. Lalvani, L. L. Kerr and H. Wang, *J. Porphyrins Phthalocyanines*, 2016, **20**, 542-555.

12 a) L. L. Li and E. W. Diau, *Chem. Soc. Rev*., 2013, **42**, 291-304; b) M. Urbani, M. Gratzel, M. K. Nazeeruddin and T. Torres, *Chem. Rev*., 2014, **114**, 12330-12396; c) N. Ma, C. Liu, Y. Qiu, S. Sun and Z. Su*, J. Comput. Chem*., 2012, **33**, 211-219; d) M. Adineh, P. Tahay, W.-K. Huang, H.-P. Wu, E. W.-G. Diau and N. Safari, *RSC Adv*., 2016, **6**, 102979-102983; e) P. A. Angaridis, E. Ferentinos, G. Charalambidis, K. Ladomenou, V. Nikolaou, S. Biswas, G. D. Sharma and A. G. Coutsolelos, *RSC Adv*., 2016, **6**, 22187-22203; f) S. Chakraborty, H.-C. You, C.-K. Huang, B.-Z. Lin, C.-L. Wang, M.-C. Tsai, C.-L. Liu and C.-Y. Lin, *J. Phys. Chem. C*, 2017, **121**, 7081-7087; g) H. H. Chou, K. S. Reddy, H. P. Wu, B. C. Guo, H. W. Lee, E. W. Diau, C. P. Hsu and C. Y. Yeh, *ACS Appl. Mater. Interfaces*, 2016, **8**, 3418-3427; h) T. Higashino, K. Kawamoto, K. Sugiura, Y. Fujimori, Y. Tsuji, K. Kurotobi, S. Ito and H. Imahori, *ACS Appl. Mater. Interfaces*, 2016, **8**, 15379-15390; i) R. Kumar, M. Sankar, V. Sudhakar and K. Krishnamoorthy, *New J. Chem*., 2016, **40**, 5704-5713; j) C. Li, L. Luo, D. Wu, R. Jiang, J. Lan, R. Wang, L. Huang, S. Yang and J. You, *J. Mater. Chem. A*, 2016, **4**, 11829-11834; k) F. Lodermeyer, R. D. Costa, J. Malig, N. Jux and D. M. Guldi, *Chem. Eur. J*., 2016, **22**, 7851-7855; l) F. Lu, J. Zhang, Y. Zhou, Y. Zhao, B. Zhang and Y. Feng, *Dyes Pigm*., 2016, **125**, 116-123; m) J. Luo, J. Zhang, K.-W. Huang, Q. Qi, S. Dong, J. Zhang, P. Wang and J. Wu, *J. Mater. Chem. A*, 2016, **4**, 8428-8434; n) S. Mathew, N. A. Astani, B. F. E. Curchod, J. H. Delcamp, M. Marszalek, J. Frey, U. Rothlisberger, M. K. Nazeeruddin and M. Grätzel, J. *Mater. Chem. A*, 2016, **4**, 2332-2339; o) X. Qian, L. Lu, Y.-Z. Zhu, H.-H. Gao and J.-Y. Zheng, *RSC Adv*., 2016, **6**, 9057-9065; p) P. Qin, P. Sanghyun, M. I. Dar, K. Rakstys, H.

ElBatal, S. A. Al-Muhtaseb, C. Ludwig and M. K. Nazeeruddin, *Adv. Funct. Mater*., 2016, **26**, 5550-5559; q) C.-L. Wang, M. Zhang, Y.-H. Hsiao, C.-K. Tseng, C.-L. Liu, M. Xu, P. Wang and C.-Y. Lin, *Energy Environ. Sci*., 2016, **9**, 200-206; r) G. Zanotti, N. Angelini, G. Mattioli, A. M. Paoletti, G. Pennesi, G. Rossi, D. Caschera, L. de Marco and G. Gigli, *RSC Adv*., 2016, **6**, 5123-5133; s) L. Zeininger, F. Lodermeyer, R. D. Costa, D. M. Guldi and A. Hirsch, *Chem. Commun*., 2016, **52**, 8842-8845.

13 Y. Hu, S. Yellappa, M. B. Thomas, R. G. W. Jinadasa, A. Matus, M. Shulman, F. D'Souza and H. Wang, *Chem. Asian. J*., 2017, **12**, 2749-2762.

14 R. Deshpande, L. Jiang, G. Schmidt, J. Rakovan, X. Wang, K. Wheeler and H. Wang, *Org. Lett*., 2009, **11**, 4251-4253.

15 a) V. Gevorgyan, N. Tsuboya, and Y. Yamamoto, *J. Org. Chem*., 2011, **66**, 2743-2746; b) F. Punner, G.Hilt, *Chem. Commun*., 2012, **48**, 3617-3619; c) S. Saito, M. M. Salter, V. Gevorgyan, N. Tsuboya, K. Tando, and Y. Yamamoto, *J. Am. Chem. Soc*., 1996, **118**, 3970-3971.

16 C.-P. Hsieh, H.-P. Lu, C.-L. Chiu, C.-W. Lee, S.-H. Chuang, C.-L. Mai, W.-N. Yen, S.-J. Hsu, E. W.-G. Diau and C.-Y. Yeh, *J. Mater. Chem*., 2010, **20**, 1127-1134.

17 K. Pei, Y. Wu, A. Islam, S. Zhu, L. Han, Z. Geng and W. Zhu, *J. Phys. Chem. C*, 2014, **118**, 16552-16561.

18 G. R. Soja and D. F. Watson, *Langmuir*, 2009, **25**, 5398-5403.

19 a) J. Bisquert, F. Fabregat-Santiago in Dye-Sensitized Solar Cells (Ed.: K. Kalyanasundaram), EPFL Press, Lausanne, Switzerland, 2010, pp. 457– 554; b) F. Fabregat-Santiago, G. Garcia-Belmonte, I. Mora-Sero, J. Bisquert, *Phys. Chem. Chem. Phys*. 2011, **13**, 9083–9118; c) M. K. Panda, G. D. Sharma, K. R. J. Thomas, A. G. Coutsolelos, *J. Mater. Chem*. 2012, **22**, 8092–8102.

20 a) H. Imahori, S. Kang, H. Hayashi, M. Haruta, H. Kurata, S. Isoda, S. E. Canton, Y. Infahsaeng, A. Kathiravan, T. Pascher, P. Chabera, A. P. Yartsev, V. Sundstrom, *J. Phys. Chem. A*. 2011, **115**, 3679-3690. b) S. Ye, A. Kathiravan, H. Hayashi, Y. Tong, Y. Infahsaeng, P. Chabera, T. Pascher, A. P. Yartsev, S. Isoda, H. Imahori, V. Sundstrom, *J. Phys. Chem. C* 2013, **117**, 6066-6080.

21 A. S. Hart, C. C. K, N. K. Subbaiyan, P. A. Karr and F. D'Souza, *ACS Appl. Mater. Interfaces*, 2012, **4**, 5813-5820.

22 A. S. Hart, B. K. Chandra, H. B. Gobeze, L. R. Sequeira, F. D'Souza, *ACS Appl. Mater. Interfaces*, 2013, **5**, 5314–5323

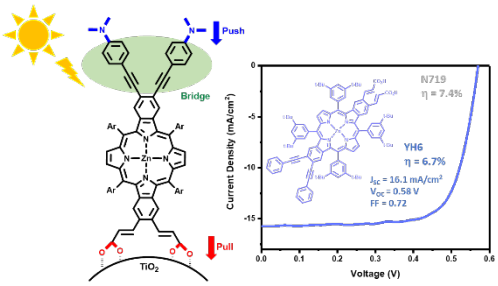

Push-pull *opp*-dibenzoporphyrins with phenylethynyl bridge were designed and synthesized as sensitizers for dye-sensitized solar cells, giving power conversion efficiency up to 6.7%, close to that of N719 dye under similar conditions.